Supporting Information

Photo-Inspired Antibacterial Activity and Wound Healing Acceleration by Hydrogel Embedded with Ag/Ag@AgCl/ZnO Nanostructures

*Congyang Mao[a], Yiming Xiang[a], Xiangmei Liu[a], Zhenduo Cui[b], Xianjin Yang[b], Kelvin Wai Kwok Yeung[c], Haobo Pan[d], Xianbao Wang[a], Paul K Chu[e], Shuilin Wu[a,b]**

[a] Hubei Collaborative Innovation Center for Advanced Organic Chemical Materials, Ministry-of-Education Key Laboratory for the Green Preparation and Application of Functional Materials, Hubei Key Laboratory of Polymer Materials, School of Materials Science & Engineering, Hubei University, Wuhan 430062, China

[b] School of Materials Science & Engineering, Tianjin University, Tianjin 300072, China

[c] Department of Orthopaedics & Traumatology, Li Ka Shing Faculty of Medicine, The University of Hong Kong, Pokfulam, Hong Kong, China

[d] Center for Human Tissues and Organs Degeneration, Shenzhen Institutes of Advanced Technology, Chinese Academy of Sciences, Shenzhen 518055, China

[e] Department of Physics and Department of Materials Science and Engineering, City University of Hong Kong, Tat Chee Avenue, Kowloon, Hong Kong, China

* To whom correspondence should be addressed:

E-mail: shuilin.wu@gmail.com; shuilinwu@tju.edu.cn (S.L. Wu)

Table of contents

1. Experimental section

1.1 Preparation of the CMC hydrogel

To prepare the CMC hydrogels in a 250 mL three-neck round bottom flask, 3 g of CMC were dissolved in 100 mL of 3% W/V NaOH under continuous stirring for 30 min to obtain a homogenous viscous mixture. 6 mL of epichlorohydrin (ECH) were added drop-wise with a funnel and stirred for 2 h until a homogenous mixture was obtained. The mixture was poured onto a glass petri dish with a diameter of 15 cm and heated to 80 ^{o}C for 2 h to achieve better prepolymerization. The prepolymer was collected and washed several times with distilled water to remove residual NaOH and ECH and dried in an oven at 50 ^{o}C for 24 h until a white solid dried gel was obtained.

1.2 Fabrication of the Ag/Ag@AgCl/ZnO embedded hydrogels

The obtained dried gel was cut with a mold to obtain slices with a regular shape and uniform size of $\phi 18\,mm \times 1\,mm$ (0.12 g). The samples were immersed in 100 mL of distilled water for 12 h for water-absorption swelling to open the pores in the gel. The swollen gel samples were immersed in 100 mL of silver nitrate ($AgNO_3$) with different concentrations (0.00, 2.50 mM, 0.75 mM, 1.25 mM, and 2.50 mM) to incorporate Ag^+ and part of Ag^+ combined with Cl^- in the hydrogels to form silver chloride (AgCl). In order to load Zn^{2+}, the swollen hydrogel plate was put in 100 mL of zinc nitrate ($Zn(NO_3)_2$) with a concentration of 5 mM for 12 h. The hydrogel samples were divided into six groups, group 1, group 2, group 3, group 4, group 5, and group 6 with 3 samples in each group. The samples were rinsed with distilled water thoroughly to remove Ag^+ and Zn^{2+} attached to the surface. After cleaning, group 1 was freeze-dried overnight to obtain the dry gel. Group 6 was placed in 100 mL of 0.01 M NaOH for 4 h to obtain ZnO produced by combination of the hydroxide ion and loaded Zn^{2+} and this group was rinsed with distilled water to remove residual

NaOH and freeze-dried overnight to obtain the dry ZnO nanocomposite hydrogels. The other 4 groups (2, 3, 4, and 5) were illuminated with UV light (λ = 365 nm) for 2 h to obtain Ag NPs from reduction of the loaded Ag^+ and AgCl. Group 2 was freeze-dried overnight to obtain the dry Ag/Ag@AgCl nanocomposite hydrogels. Groups 3, 4, and 5 were placed in 100 mL of 5 mM of $Zn(NO_3)_2$ for 12 h and the subsequent processes were the same as that for group 6 followed by freeze-drying overnight to obtain the dry Ag/Ag@AgCl/ZnO nanocomposite hydrogels. The products were labeled as H1, H2, H3, H4, H5, and H6 as shown in Table S1.

1.3 Characterization of the nanocomposite hydrogels

To determine the phase structure, the dried gels with different concentrations of initial $AgNO_3$ were analyzed by X-ray diffraction (XRD, D8A25, Bruker, Germany) in the continuous mode with 2θ scanned from 20^o to 80^o, step size of 0.02^o, and incident angle of 3^o. The morphology and composition of the dried gels were determined by a scanning electron microscopy (SEM, JSM7100F and JSM6510LV) equipped with an energy-dispersive X-ray spectrometer (EDS). The microstructure of the dried gels was investigated by transmission electron microscope (TEM, Tecnai G20) and selected-area electron diffraction (SAED).

1.4 Swelling behavior

To facilitate the swelling tests and biological assay, the samples (H1, H2, H3, H4, H5, and H6) were cut into circular pieces with dimensions of $\phi 5mm \times 2mm$ (0.7 mg). The samples were immersed in 10 mL of aqueous solutions with a series of pH at room temperature for 24 h to reach the swelling equilibrium. The swelling ratio of the hydrogels was calculated by Eq. (1).

$$\text{Swelling ratio} = \frac{(W - W_0) * 100\%}{W_0} \quad (1),$$

where W_0 was the initial weight of the dried gels and W was the weight of the samples after swelling for 24 h. To prepare the different pH media, the HCl (1.0 M) and NaOH (1.0 M) solutions were diluted with distilled water to reach the pre-designated pH of 2, 3, 4, 5.6, 7, 8, 9, or 10.

2. Results and discussion

2.1 Swelling behavior

The swelling ratios of all hydrogels increase as the pH goes up from 2 to 8 but decreases when the pH is over 8. This is caused by the carboxylate groups on the polymer chains being protonated at a low pH to eliminate the anion-anion repulsive forces. Water molecules are taken out to decrease the swelling ratio. When the pH reaches 8, the carboxylate groups are ionized resulting in electrostatic repulsion between the carboxylate groups and the maximum swelling capacity. However, in the more basic solutions (pH = 9 and 10), the ionic strength of the medium increases and as a result, the carboxylate groups are shielded by the counter ions from the solution thus preventing electrostatic repulsion and decreasing the swelling ratio.

The swelling ratio of H6 is less than that of H2 at low pH (< 6) due to ZnO NPs in H6. When the ZnO NPs are dissolved in the acidic solutions, they produce a large number of zinc ions and part of Zn^{2+} with two positive charges is bound to two carboxylate groups on the adjacent two chains as shown in Figure S7a. This produces compressing force between the two chains to decrease the swelling ratio. The force is eliminated when the pH is over 7 because the ZnO NPs remaining in the solutions produce a larger swelling ratio for H6 than H2. As shown in Figure S7b, the CMC hydrogel swells after water absorption but shrinks in the presence of Zn^{2+}. The corresponding optical images in Figure S7c provide further evidence about this phenomenon. The diameter of the hydrogel increases from 5 mm to 17 mm after water absorption but

decreases to 13 mm in the presence of Zn^{2+}. The Zn^{2+} response makes it possible for the CMC hydrogel to be a special carrier in drug delivery systems. Furthermore, the corresponding optical images in Figure S8 illustrate the rapid reversible swelling-shrinking behavior of the hydrogels, indicating that they are promising in drug delivery systems, tissue engineering, sensing systems, smart coating materials, and so on.[1-3]

2.2 Effects of light intensity and wavelength on the antibacterial activity

H2 is selected to study the effects of light intensity and wavelength on the antibacterial activity due to its excellent photocatalytic property. As shown in Figure S16A, as the visible light intensity is increased, the number of colony units decreases and the antibacterial ratio of H2 increases gradually (Figure S16B). Moreover, H2 delivers excellent antibacterial performance after irradiation with a 200 W xenon lamp with wavelengths over 300 nm or over 410 nm (controlled by the optical filter) as shown in Figure S17. The antibacterial effect of H2 diminishes when the wavelength is larger than 510 nm, especially over 600 nm and over 800 nm, indicating that light with the wavelength range of 300-510 nm is crucial to the antimicrobial and photocatalytic activity of the Ag/Ag@AgCl hybrid nanostructures (H2).

2.3 SEM images of the hydrogel after wound therapy

The SEM images of the Ag/Ag@AgCl/ZnO nanocomposite hydrogels after wound healing in the animal models are depicted in Figure S21. The Ag@AgCl nanostructures (Figure S21A) are still intact while both Ag and ZnO are reduced sharply and even disappear due to the acidic environment arising from inflammation during the wound healing process. Both the Ag NPs and ZnO can dissolve in the acidic environment and it is consistent with the ion release behavior presented in

Figure 3.

3. Supplementary Table and Figures

	Step 1	Step 2	Step 3	Step 4	Step 5
H1	H_2O 12 h	—	—	—	—
H2	H_2O 12 h	$AgNO_3$ 2.5 mM 12 h	UV 2 h	—	—
H3	H_2O 12 h	$AgNO_3$ 0.75 mM 12 h	UV 2 h	$Zn(NO_3)_2 \cdot 6H_2O$ 5 mM 12 h	NaOH 0.01 M 4 h
H4	H_2O 12 h	$AgNO_3$ 1.25 mM 12 h	UV 2 h	$Zn(NO_3)_2 \cdot 6H_2O$ 5 mM 12 h	NaOH 0.01 M 4 h
H5	H_2O 12 h	$AgNO_3$ 2.5 mM 12 h	UV 2 h	$Zn(NO_3)_2 \cdot 6H_2O$ 5 mM 12 h	NaOH 0.01 M 4 h
H6	H_2O 12 h	$Zn(NO_3)_2 \cdot 6H_2O$ 5 mM 12 h	NaOH 0.01 M 4 h	—	—

Table S1. Fabrication process for the different nanocomposite hydrogels.

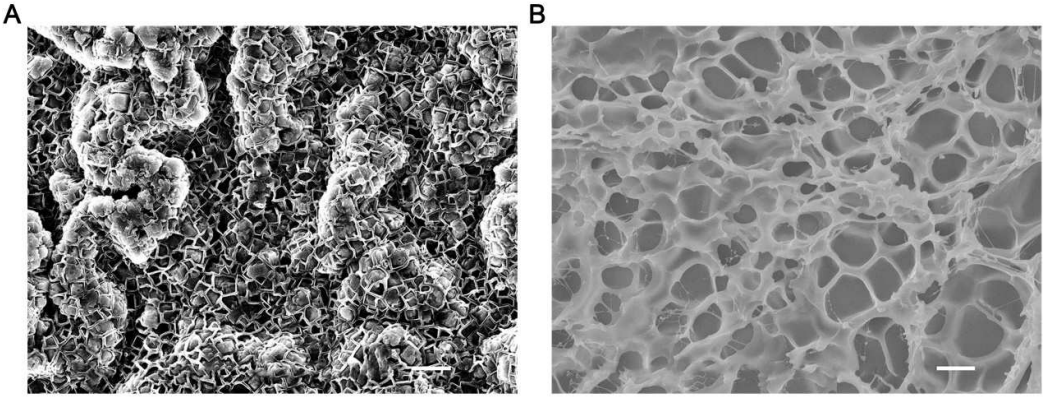

Figure S1. Typical SEM images of the networks in the CMC hydrogel of (A) not swollen and (B) Swollen after water absorption (Scale bars = 10 μm).

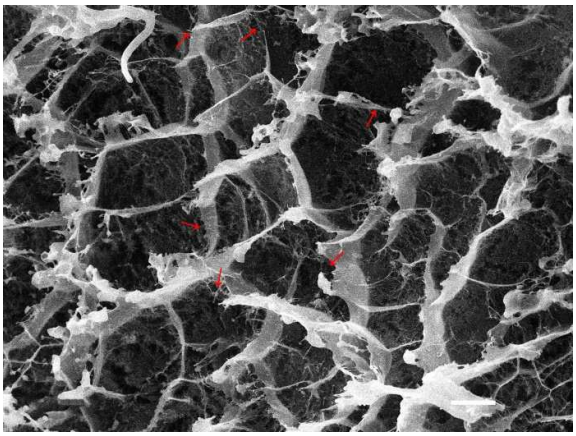

Figure S2. SEM images of the damaged networks in the CMC hydrogel (Scale bar = 10 μm).

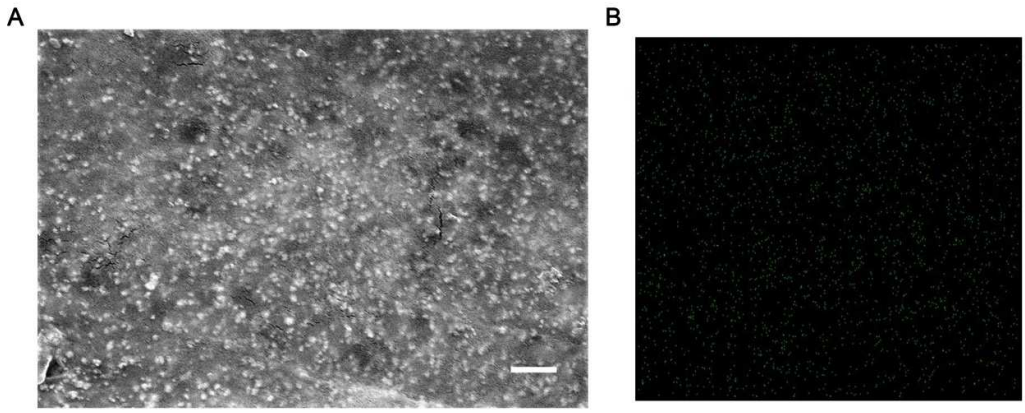

Figure S3. SEM images of (A) Ag nanoparticles in hydrogel and (B) Corresponding elemental area scan by EDS (Scale bar = 1 μm).

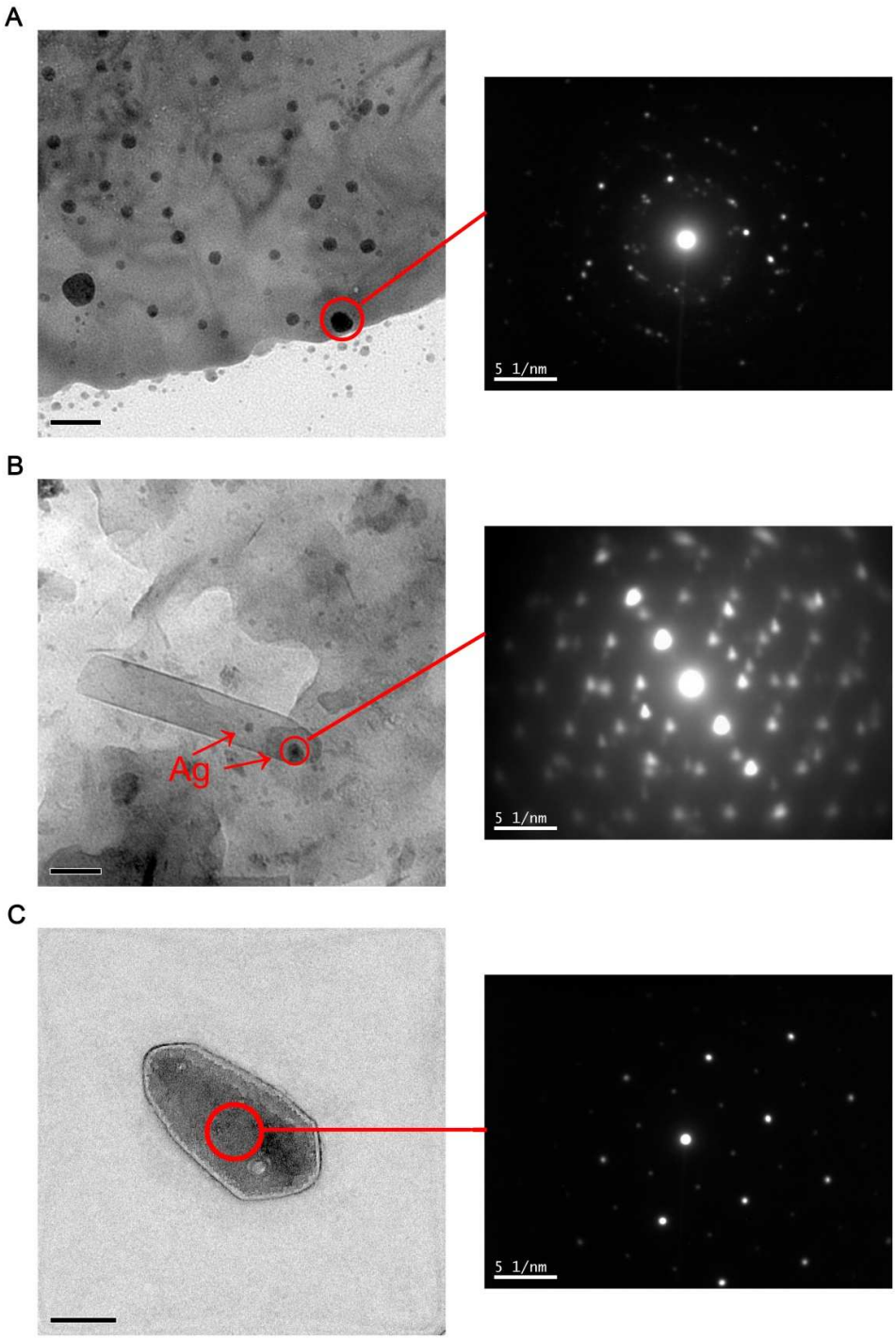

Figure S4. TEM image of (A) Ag nanoparticles, (B) Ag nanoparticles incorporated into the ZnO nanorods (Scale bars = 50 nm.), and (C) ZnO nanoparticles in the hydrogels. The insets are the corresponding SAED results (Scale bar = 100 nm).

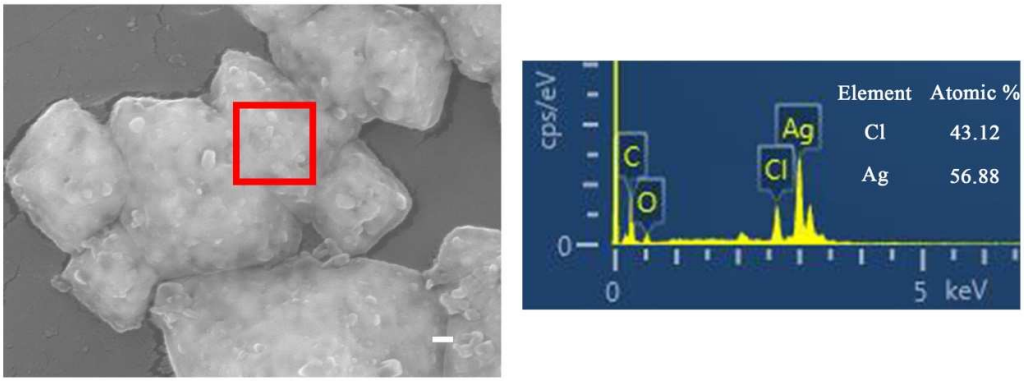

Figure S5. EDS analysis of Ag@AgCl nanostructures (Scale bar = 100 nm).

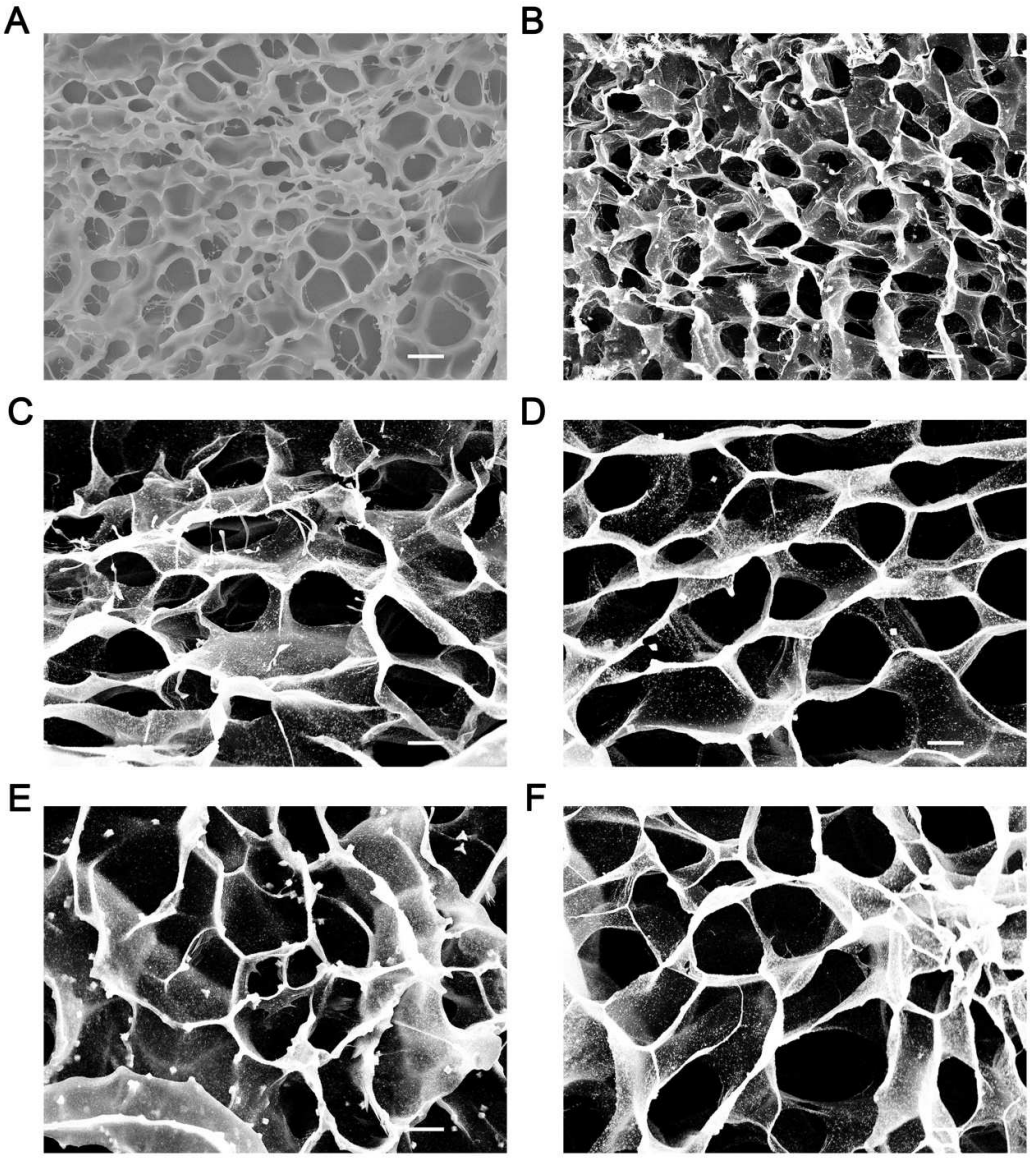

Figure S6. Typical SEM images of the networks in the hydrogels of (A) H1, (B) H2, (C) H3, (D) H4, (E) H5 and (F) H6 (Scale bars = 10 μm).

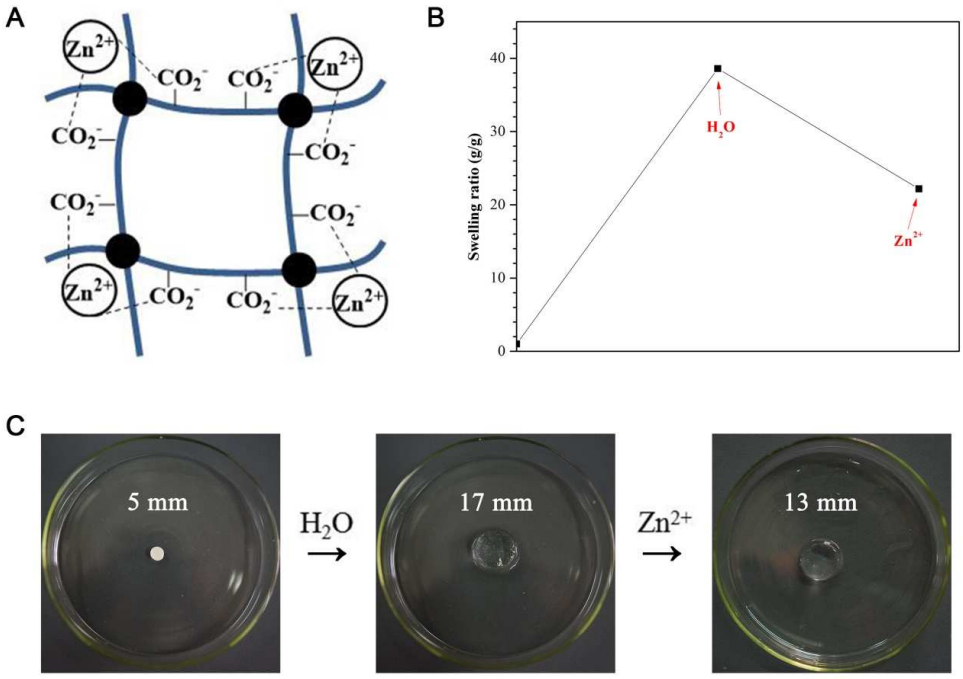

Figure S7. (A) Combination of Zn^{2+} with the networks of hydrogel, (B) Zn^{2+} responsive swelling, and (C) Corresponding optical images.

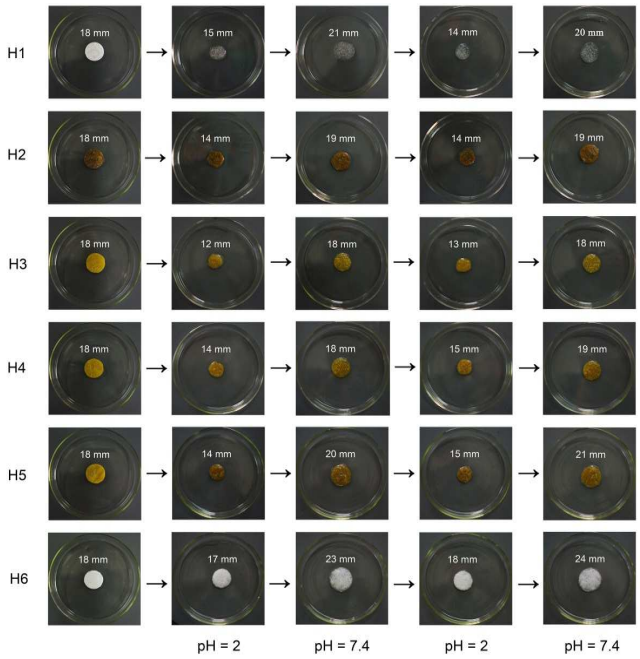

Figure S8. Optical images corresponding to the cyclic pH-stimulated transitions of hydrogels between pH changes from 2 to 7.4 with 1-min intervals.

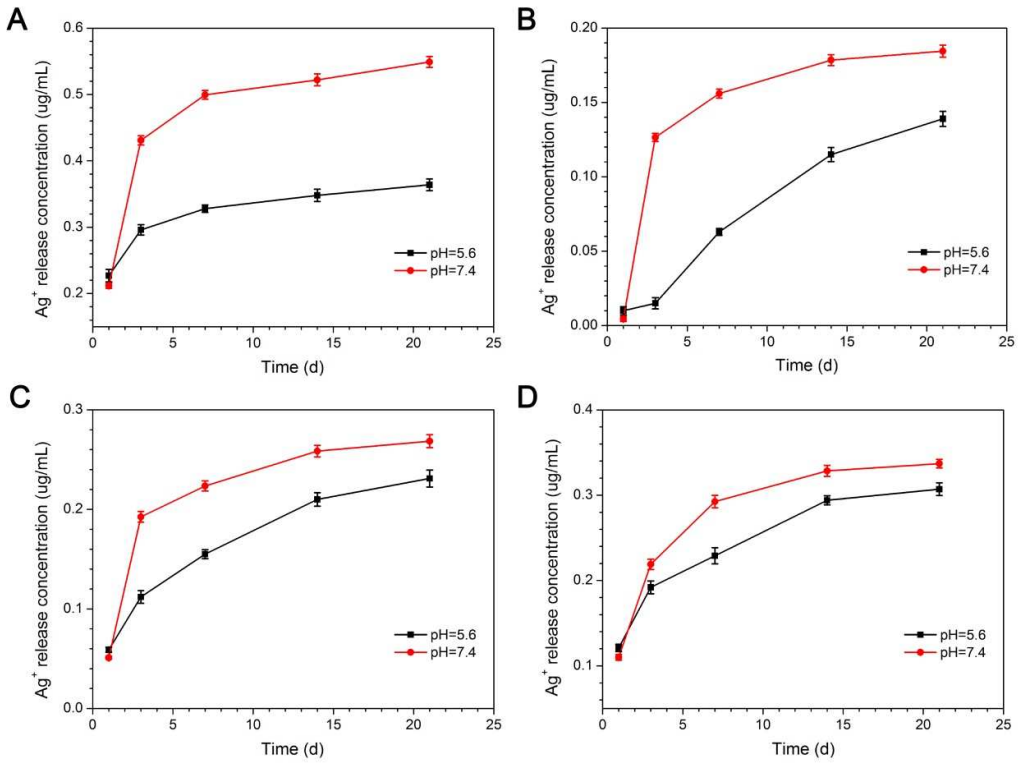

Figure S9. Cumulative silver ion release profiles acquired from the nanocomposite hydrogels: (A) H2, (B) H3, (C) H4 and (D) H5 in pH 7.4 and 5.6 PBS. The experiment was performed in triplicate and independently (n = 3) with data being mean ± SD.

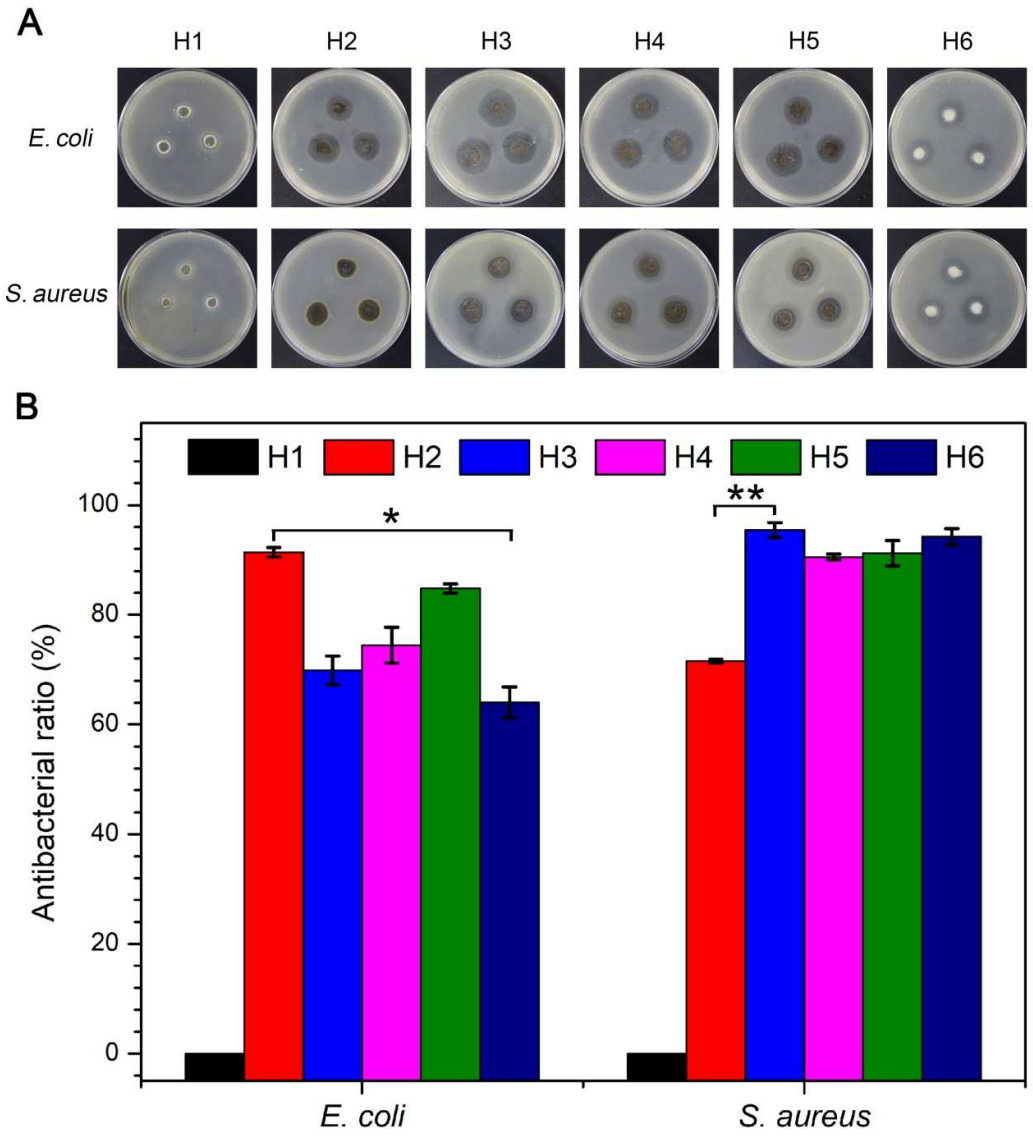

Figure S10. (A) Formed inhibition zones of swollen hydrogels of H1, H2, H3, H4, H5, and H6 against *E. coli* and *S. aureus* after incubation at 37°C in darkness for 12 h for *E. coli* and 24 h for *S. aureus*; (B) Antibacterial effects of the ions released from the different samples in darkness for 12 h for *E. coli* and 24 h for *S. aureus*. The experiment was performed in triplicate and independently (n = 3) with data being mean ± SD.

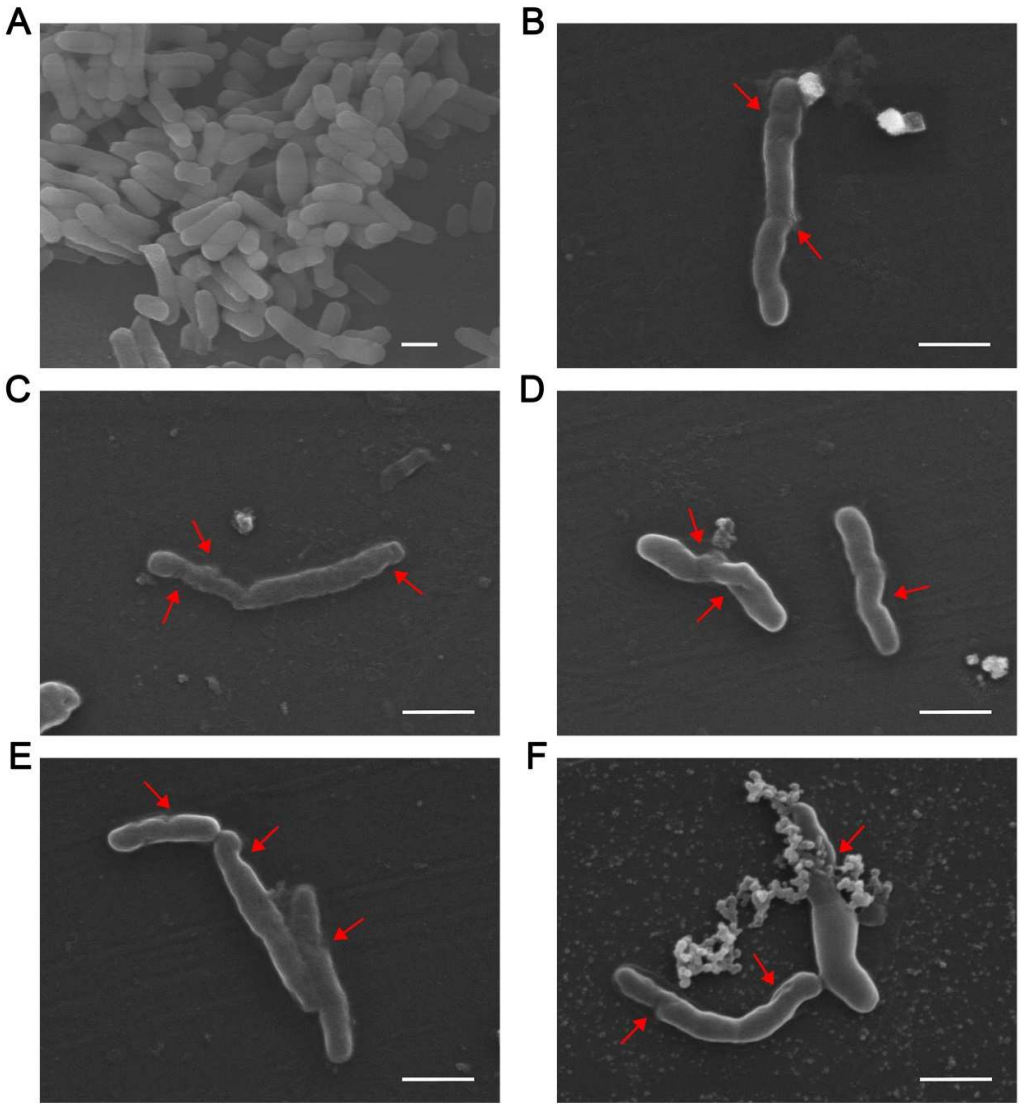

Figure S11. SEM images of *E. coli* treated with (A) H1, (B) H2, (C) H3, (D) H4, (E) H5 and (F) H6 (Scale bars = 1 μm).

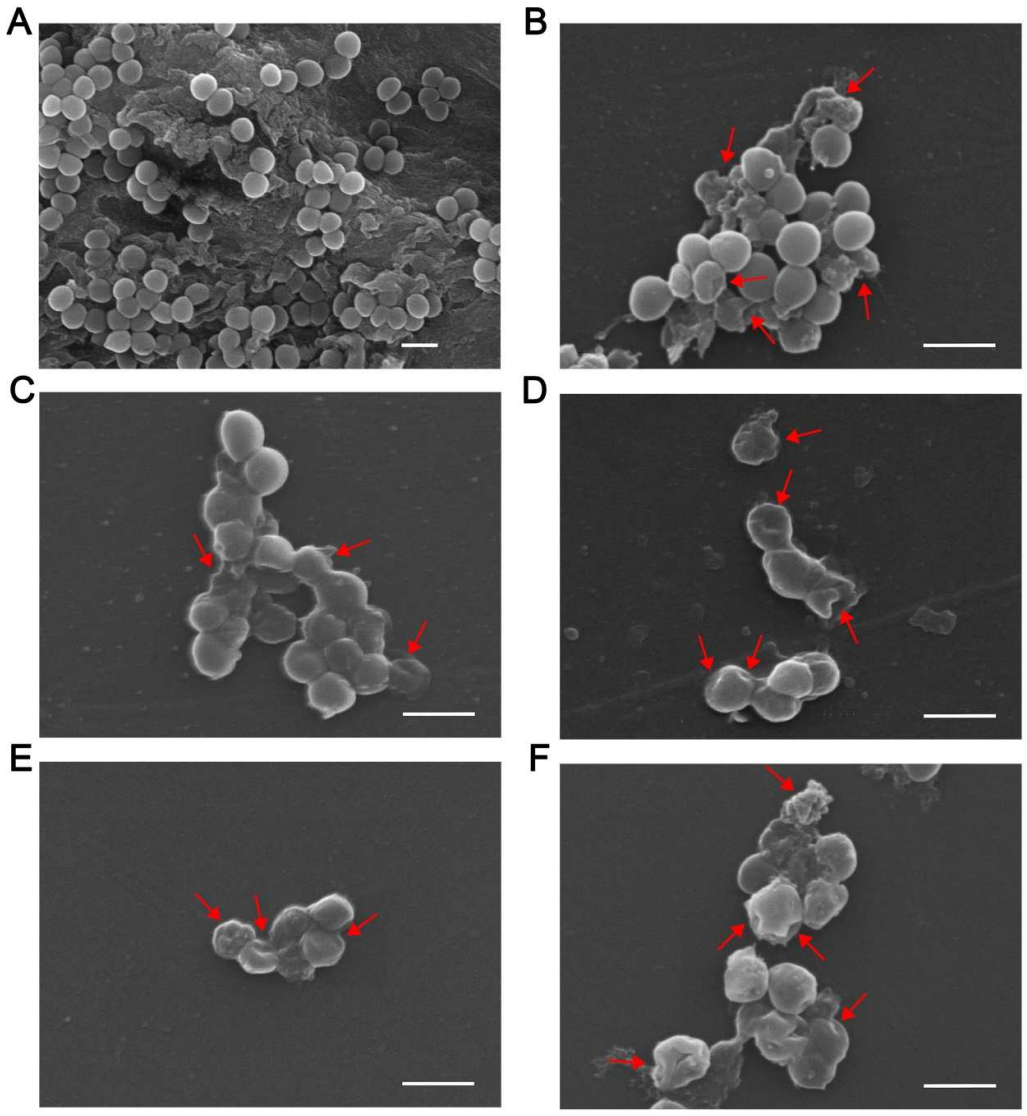

Figure S12. SEM images of *S. aureus* treated with (A) H1, (B) H2, (C) H3, (D) H4, (E) H5 and (F) H6 (Scale bars = 1 μm).

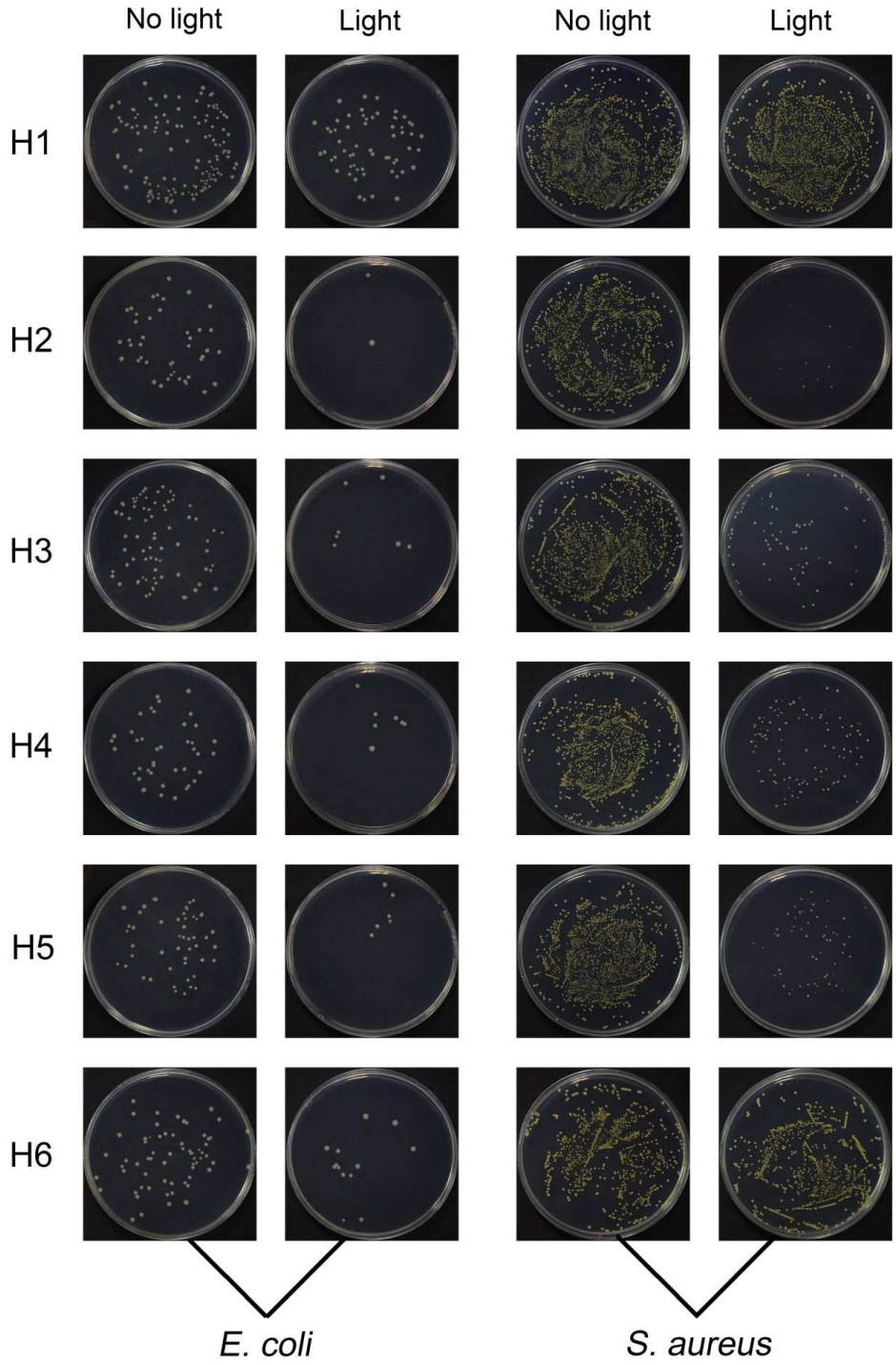

Figure S13. Formed viable colony units of *E. coli* (left) and *S. aureus* (right) after treatment with hydrogels under visible light or without light for 20 min, incubated at 37 °C in darkness for 1 hour, diluted 200 times, spread on LB agar plates, and incubated at 37 °C for 24 h.

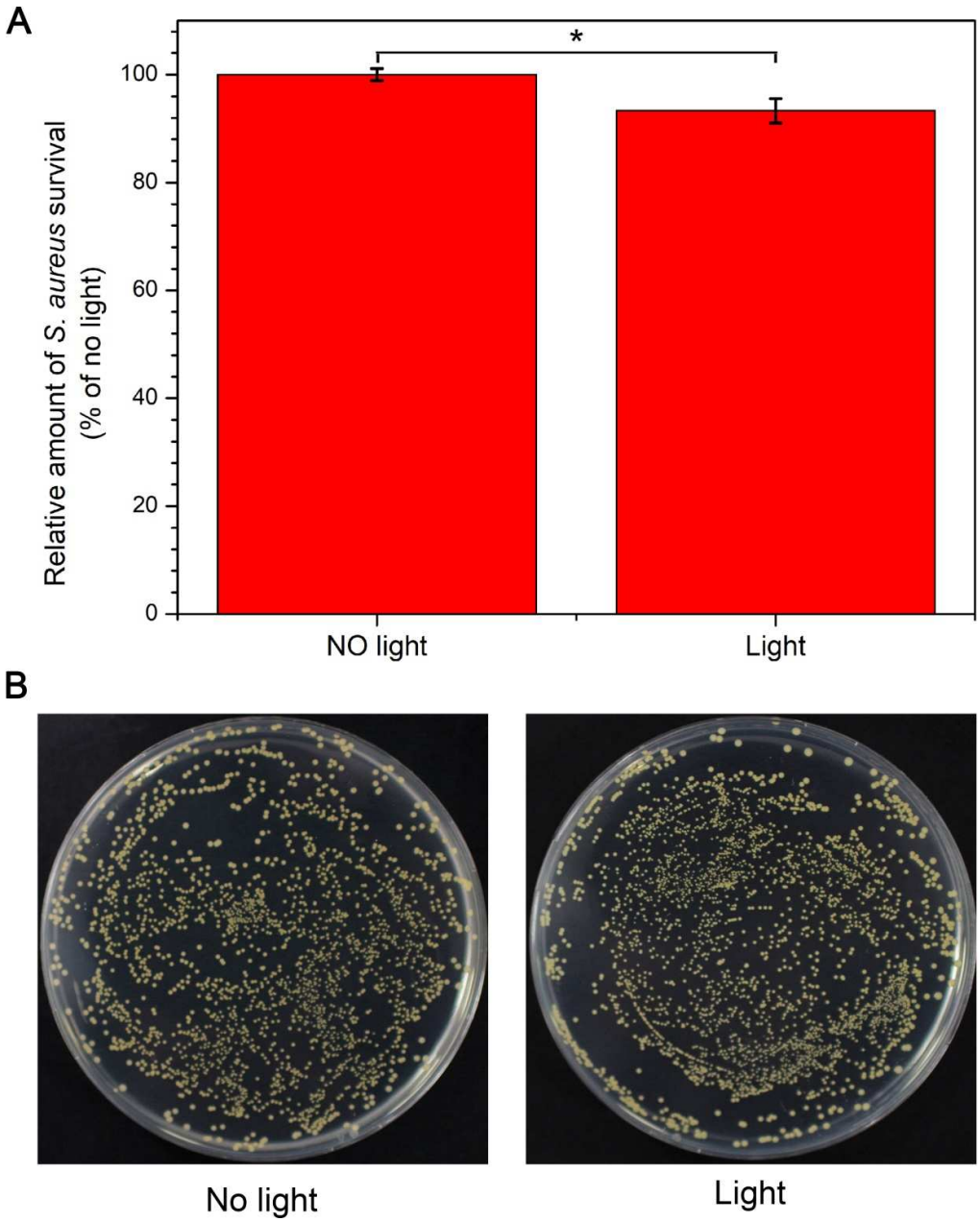

Figure S14. (A) Survival ratios of *S. aureus* before and after light illumination; **(B)** Corresponding formed viable colony units. The experiment was performed in triplicate and independently (n = 3) with data being mean ± SD.

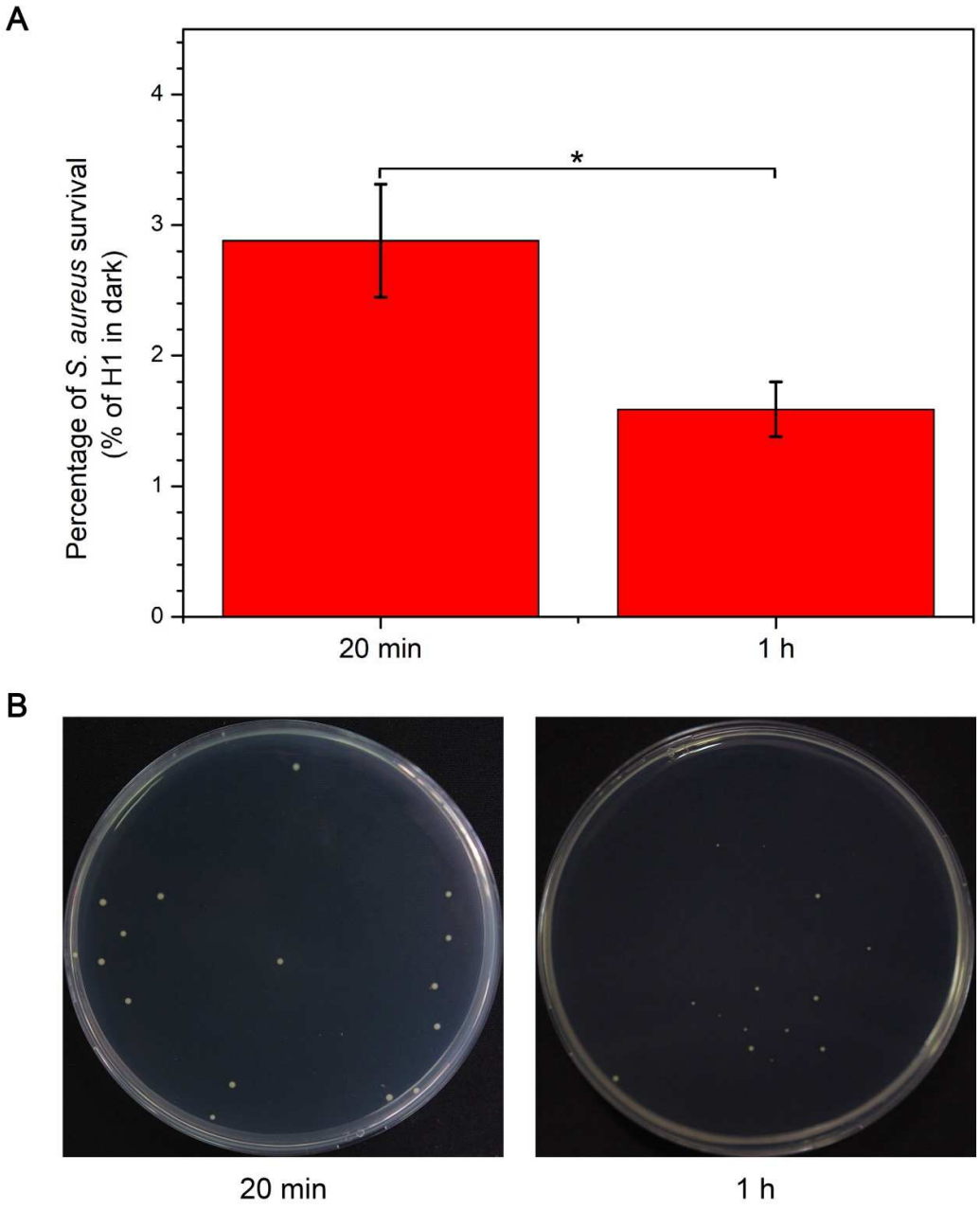

Figure S15. (A) Survival ratios of *S. aureus* after exposure to H2 and simulated sunlight for only 20 min and for 20 min (with 1 h in darkness); (B) Corresponding formed viable colony units. The experiment was performed in triplicate and independently (n = 3) with data being mean ± SD.

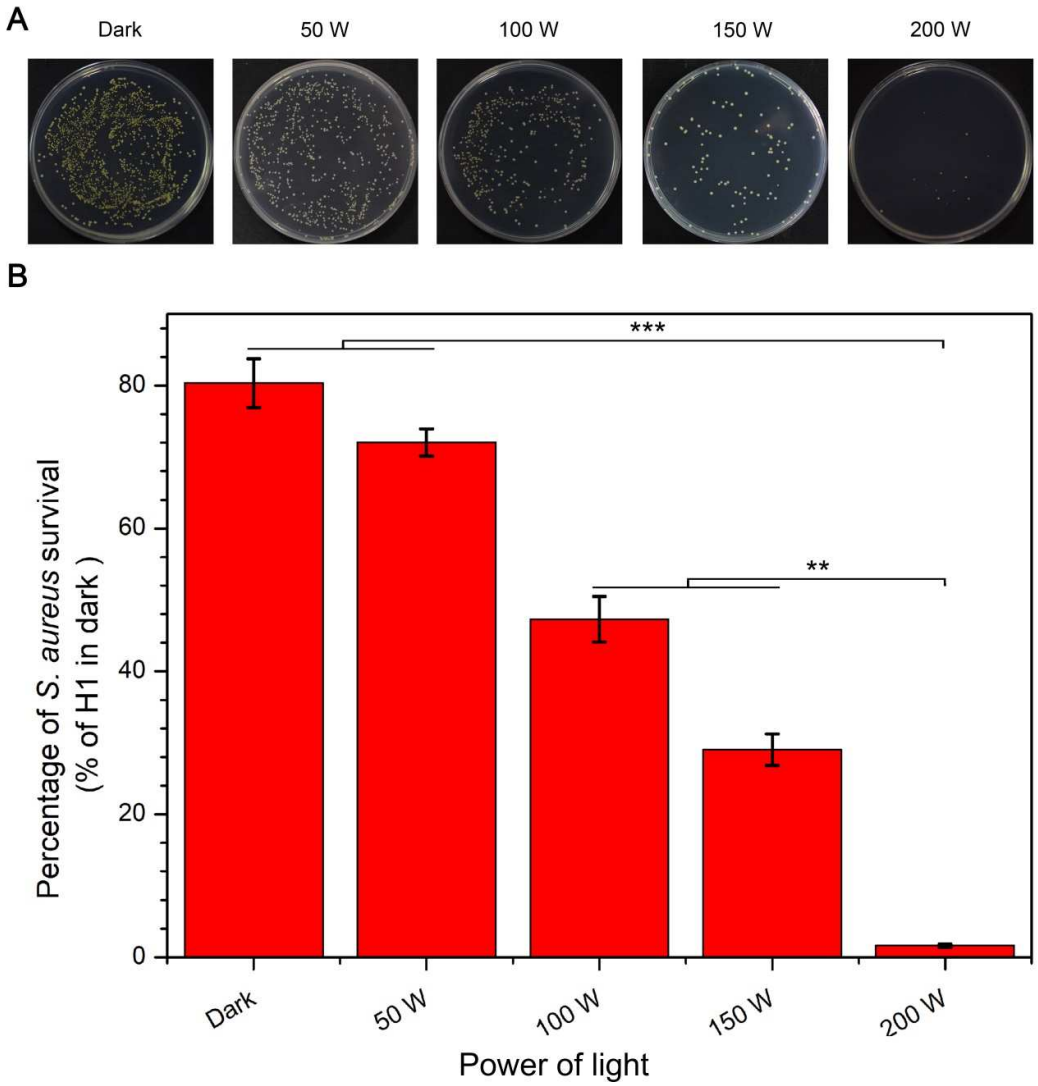

Figure S16. (A) Formed viable colony units of *S. aureus* after exposure to H2 and simulated sunlight with different power for 20 min (with 1 h in darkness); (B) Corresponding survival ratios. The experiment was performed in triplicate and independently (n = 3) with data being mean ± SD.

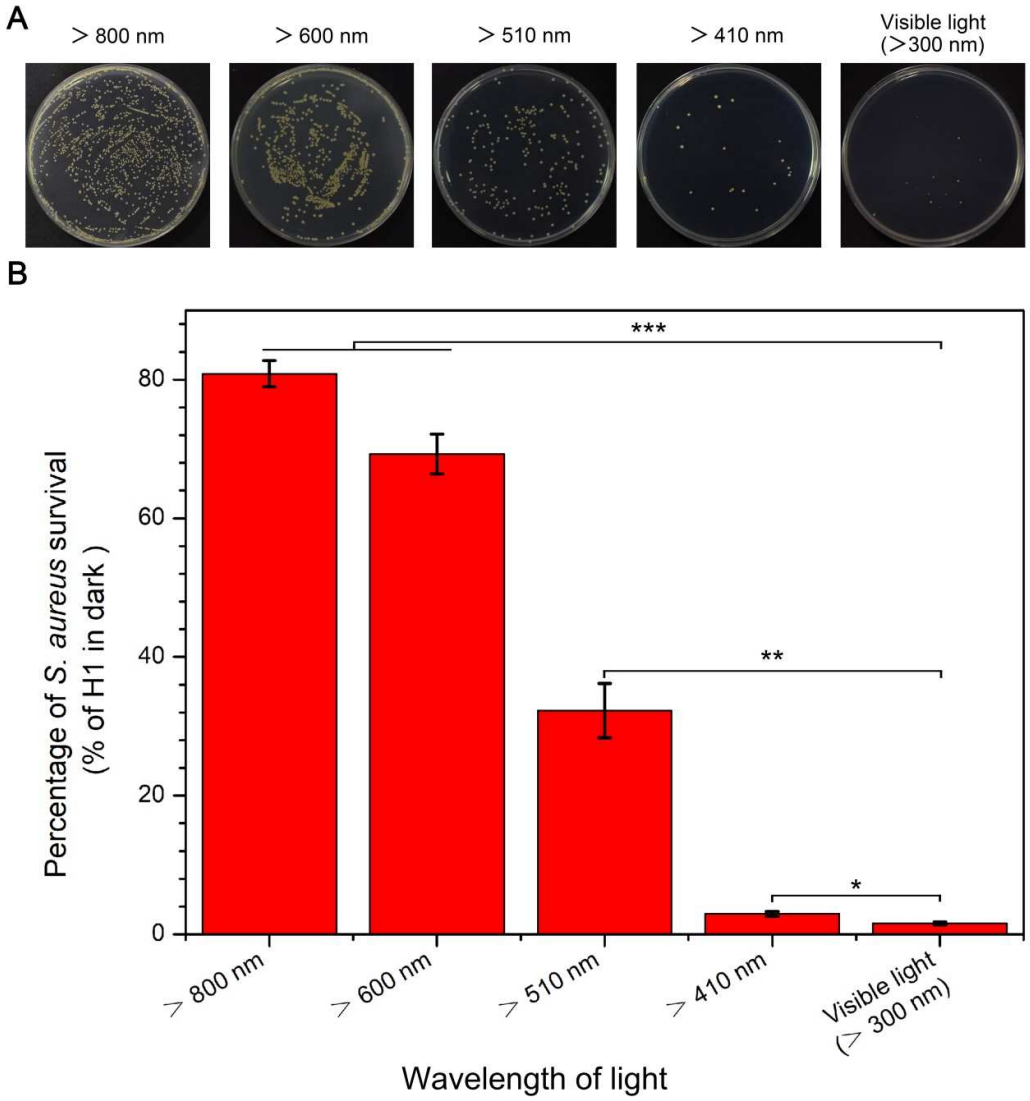

Figure S17. (A) Formed viable colony units of *S. aureus* after exposure to H2 and different wavelengths for 20 min (with 1 h in darkness); (B) Corresponding survival ratios. The experiment was performed in triplicate and independently (n = 3) with data being mean ± SD.

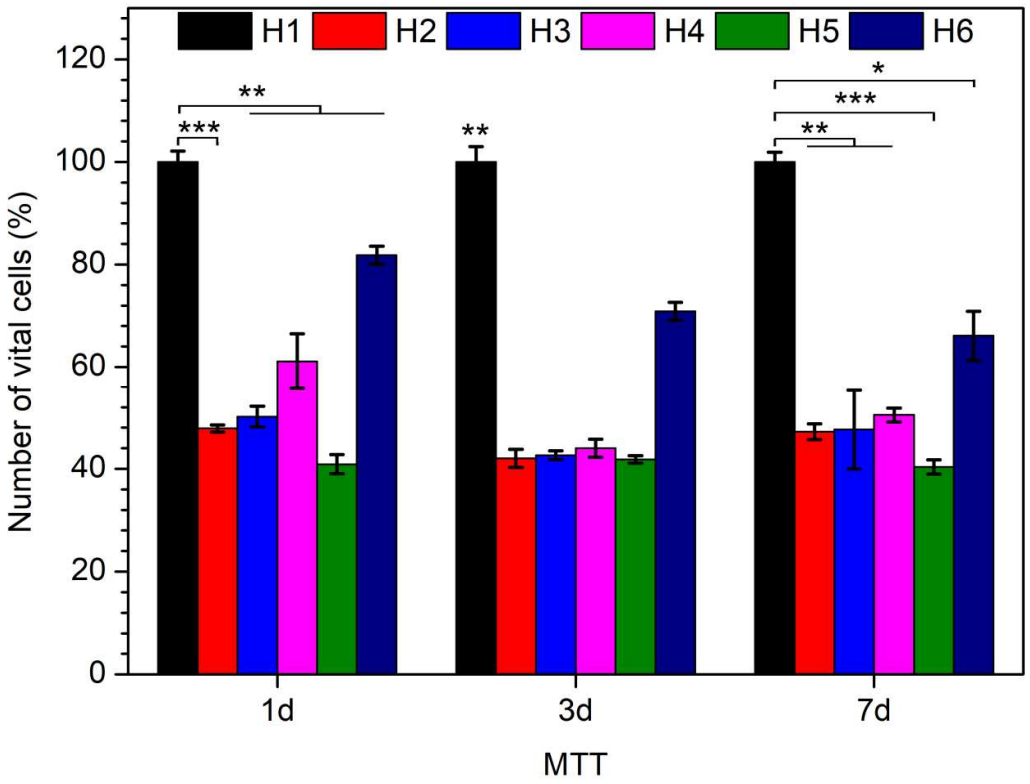

Figure S18. Cell viability treated with the hydrogels at days 1, 3 and 7. The experiment was performed in triplicate and independently (n = 3) with data being mean ± SD.

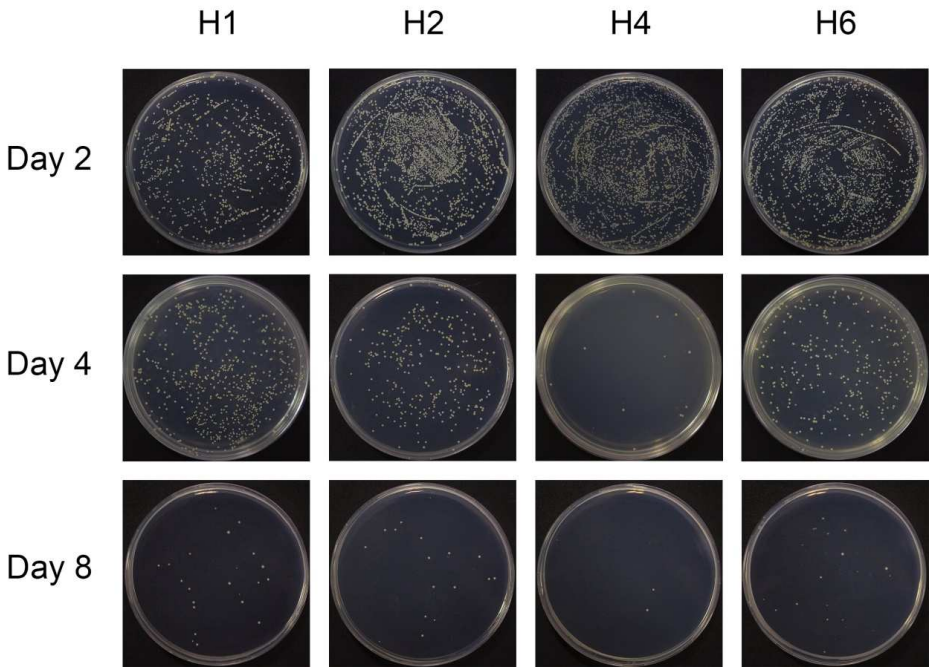

Figure S19. Viable colony units of *S. aureus* formed from the exudate of the wounds at days 2, 4 and 8.

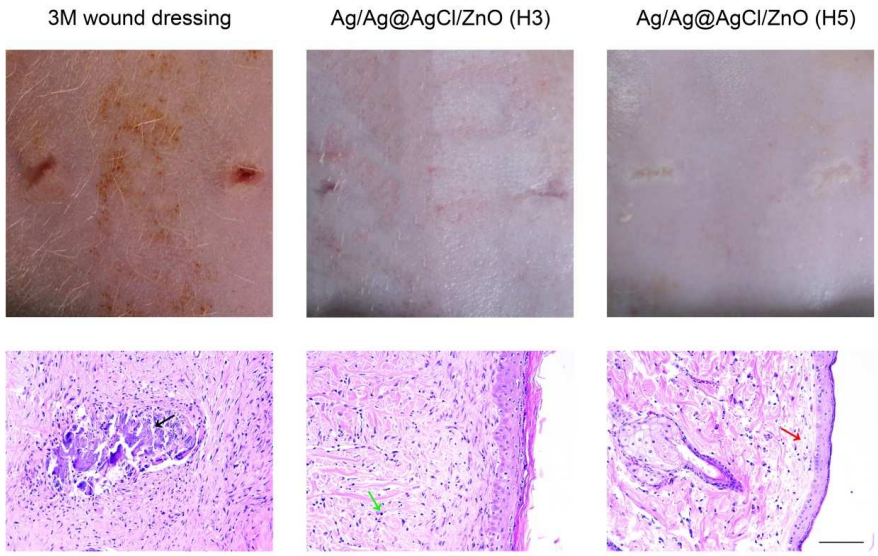

Figure S20. Wound photographs taken from the rats after 14-day treatment by 3M wound dressing, H3, and H5 and the corresponding immunology of histological images of the skin tissue samples on the wounds (Scale bar = 100 μm).

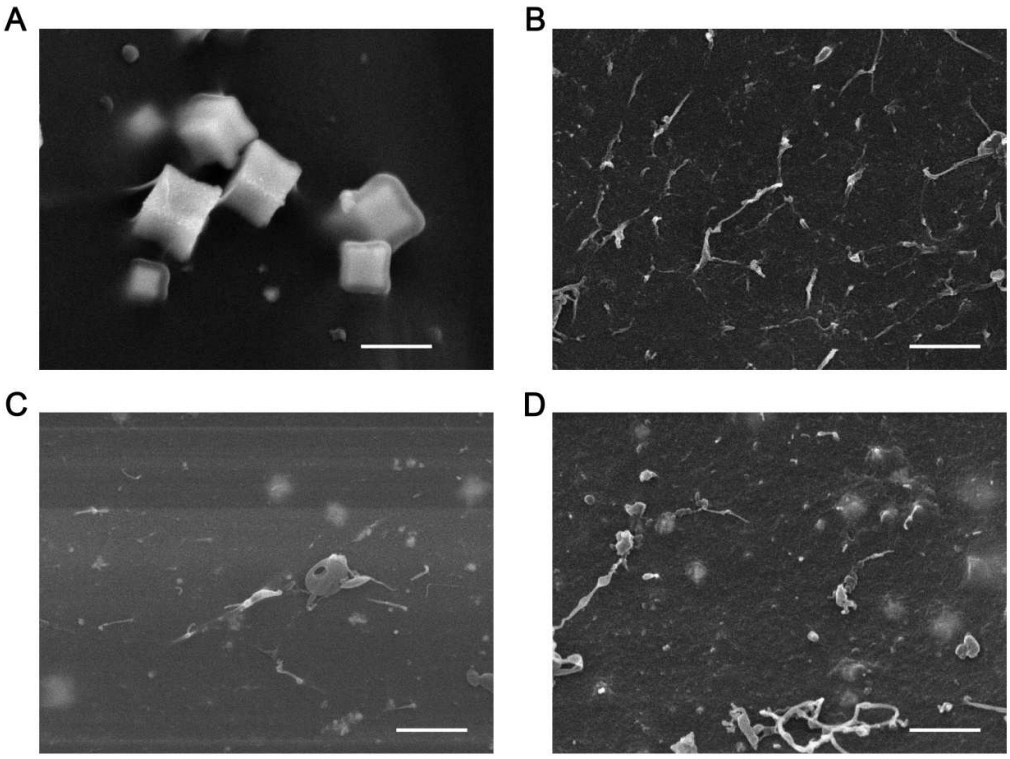

Figure S21. SEM images of (A) Ag/Ag@AgCl nanostructures, (B) H3, (C) H4, and (D) H5 after wound healing in the animal models (Scale bar = 1 μm).

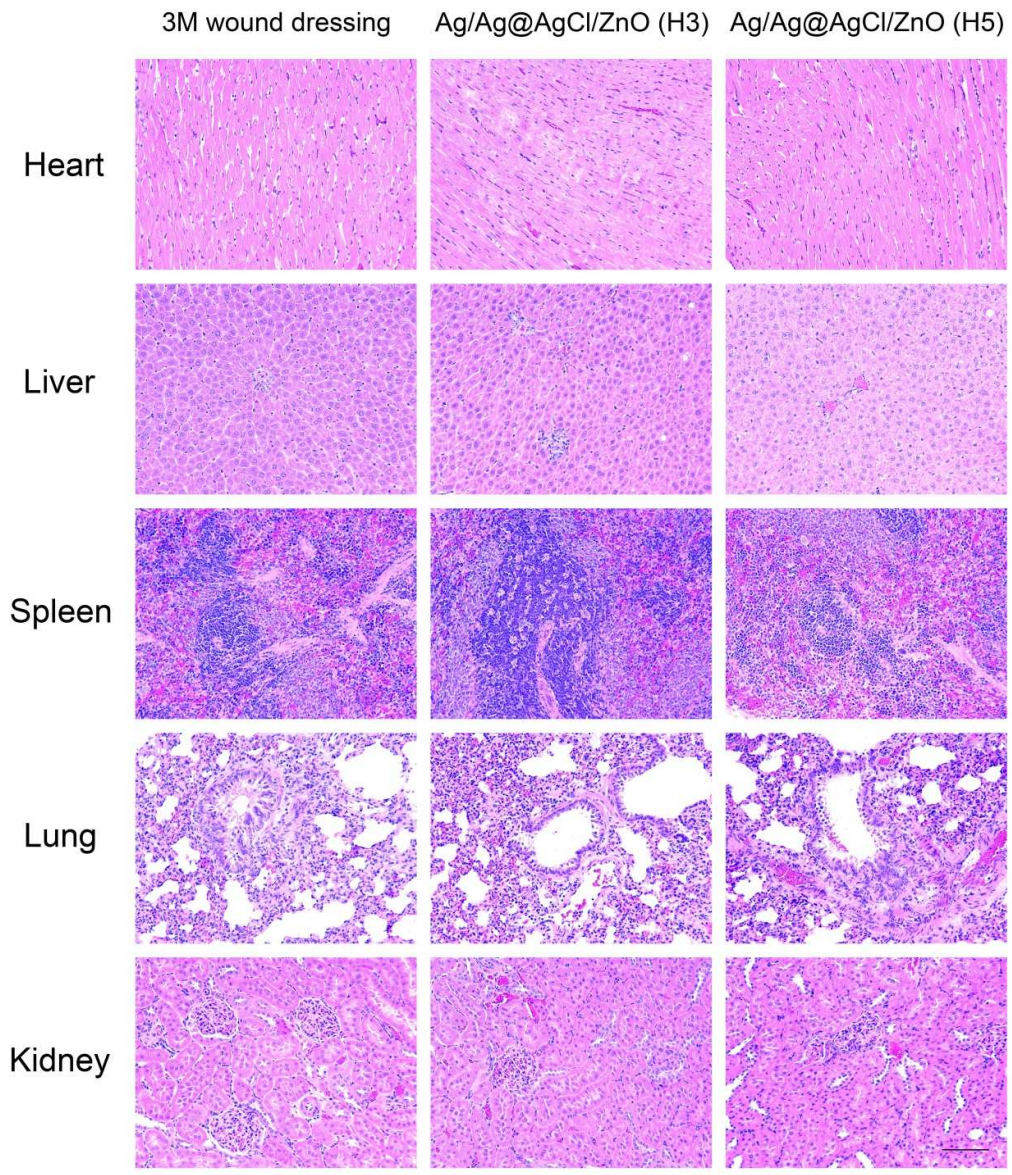

Figure S22. H&E staining of the heart, liver, spleen, lung, and kidney tissue slices after the 14-day treatment for different treatment groups (3M wound dressing, H3, and H5) [Scale bar = 100 μm].

4. References

1. Hu, Y.; Lu, C. H.; Guo, W.; Aleman-Garcia, M. A.; Ren, J.; Willner, I. A Shape Memory Acrylamide/DNA Hydrogel Exhibiting Switchable Dual pH-Responsiveness. *Adv. Funct. Mater.* **2015**, *25*, 6867—6874.

2. Guo, W.; Lu, C. H.; Orbach, R.; Wang, F.; Qi, X. J.; Cecconello, A.; Seliktar, D.; Willner, I. pH-Stimulated DNA Hydrogels Exhibiting Shape-Memory Properties. *Adv. Mater.* **2015**, *27*, 73—78.

3. Ren, J.; Hu, Y.; Lu, C. H.; Guo, W.; Aleman-Garcia, M. A.; Ricci, F.; Willner, I. pH-Responsive and Switchable Triplex-Based DNA Hydrogels. *Chem. Sci.* **2015**, *6*, 4190—4195.